Heliyon 9 (2023) e20510

Contents lists available at ScienceDirect

Heliyon

journal homepage: www.cell.com/heliyon

Construction of novel potentiometric sensors modified with biogenically synthesized metal oxide nanoparticles for sensitive detection of the opioid agonist-antagonist nalbuphine hydrochloride in its injection

Seham S. Alterary

Department of Chemistry, College of Science, King Saud University, P.O. Box 22452, Riyadh, 11495, Saudi Arabia

ARTICLE INFO

Keywords:
Nanocatalysts
Metal oxides nanoparticles
Green synthesis
Opioid agonist/antagonists
Sensing materials
Nalbuphine hydrochloride

ABSTRACT

Novel and sensitive potentiometric sensors were described for the assay of nalbuphine HCl (NBP) in authentic powder and injection samples. The developed sensors were modified with alumina nanoparticles (Al_2O_3NPs) and copper oxide nanoparticles (CuONPs). The nanoscale materials were synthesized using the extract of *Salvia officinalis* leaves in an environmentally friendly manner. The synthesized metal oxides were fully confirmed by various analytical techniques. Scanning electron microscope confirmed the morphology of nanosized materials with even distribution and particle size of 55.07 ± 4.15 and 59.48 ± 4.50 nm for Al_2O_3NPs and CuONPs, respectively. The modified sensors were prepared in three different steps. Nalbuphine hydrochloride was mixed with phosphomolybdic acid to prepare the sensor material nalbuphine phosphomolybdate (NBP-PM). It was then mixed with polyvinyl chloride in the presence of *o*-nitrophenyl ether and metal oxide nanoparticles to form the membrane matrix. Finally, a copper wire was coated with the sensing material. Excellent potentials of 1.0×10^{-8}-1.0×10^{-2} and 1.0×10^{-9}-1.0×10^{-2} mol L^{-1} were measured with lower assay limits of 4.8×10^{-9} and 5.0×10^{-10} mol L^{-1}. The average detection % were 99.28 ± 0.58% and 99.52 ± 0.28% for NBP-PM-Al_2O_3NPs and NBP-PM-CuONPs, correspondingly. The suitability of the described sensors was investigated in terms of various validation criteria, and the modified sensors exposed excellent applicability and insurance for the quantification of nalbuphine hydrochloride in its bulk samples and injections compared with another standard sensor. It is obvious that the developed NBP-PM-Al_2O_3NPs and NBP-PM-CuONPs will serve as suitable sensors for the determination of NBP.

1. Introduction

In recent years, nanobiotechnology has become a fundamental branch of current science and a new era in the field of materials science, attracting worldwide interest due to its numerous applications [1]. The conventional techniques for producing nanoparticles include thermal decomposition [2], microwave synthesis [3], electrochemical synthesis [4], ultraviolet irradiation [5], laser ablation [6], laser irradiation [7], and chemical reduction method [8]. The fabrication of progressive and clean nanomaterials using several conventional probs, on the other hand, has numerous limitations, such as the use of harmful organic reagents and solvents, the need to elevate the pressure and temperature, and the release of toxic and detrimental byproducts, all of which cause environmental issues

E-mail address: salterary@ksu.edu.sa.

https://doi.org/10.1016/j.heliyon.2023.e20510
Received 16 July 2023; Received in revised form 19 September 2023; Accepted 27 September 2023
Available online 28 September 2023

[9–11].

Various nanoparticles have been produced by biosystems [12–18]. The preparation of nanoparticles using extracts of plants considered a successful strategy to develop a fast, hygienic, non-toxic, and ecologically aware technology. The nanomaterials production such as using plants biomass would be of greater importance if they were produced unique phase and size distribution. Due to the wide diversity of their extracts, the usefulness activity for the production of these metal oxide NPs remains to be investigated [19].

Salvia officinalis (Sage) is a subshrub with purple-blue flowers and grayish leaves. It is native to the Mediterranean region, but has grown in numerous areas worldwide. It is traditionally used for medical treatments [20]. *Salvia officinalis* contains several bioactive constituents, including phenolic substances, flavonoids, and others. These phytoconstituents act as capping, stabilizing, and reducing materials and provide the necessary flexibility for more control of the nanomaterials production [21]. The literature review considered several papers describing the use of Salvia officinalis extracts in the preparation of green nanoparticles [22–24].

To produce modified polymeric sensing materials, a series of metal oxide nanoparticles were incorporated into the conductive polymer. Modified sensor materials are used in various systems including electrochemical, batteries, and biosensors, etc. [25–31].

Alumina (Al_2O_3NPs) is one of the most impact metal oxides [32,33]. They can be handled and accessed in the same way as other metal oxide nanoparticles. Moreover, these low-cost nanoparticles have a large surface area and mechanical strength [34–36]. In addition, the outstanding optical capabilities of alumina nanoparticles are used as a model for studying the properties of nanomaterials and structural and electrical changes. Due to their bio-inertness and easy surface functionalization, they can also be used in biological environments [37].

Copper oxide nanoparticles (CuONPs) are p-type semiconductors. It is a monoclinic crystalline structure metal oxide with phase and a number of impact features such as excellent thermal conductivity, high stability, and antipathogenic potential. CuO has been investigated for various purposes due to its exceptional properties, magnetic applications, sensors, and catalysis [38–41].

Al_2O_3 and CuO nanoform have unique advantages such as electrochemical activity, chemical stability, large and specific surface area, and high electron communication features [42]. Owing to their extraordinary electrochemical activities and the probability of enhanced electron transfer at low potential, Al_2O_3 and CuONPs are excellent candidates for sensing applications [43–48].

Generally, membranes matrix prepared from polyvinyl chloride with fluidizing substance as solvents are used. These membranes have lipophilic ions that operate as active materials, causing particular interaction between analytes in the membrane sections, permitting the sensor to determine them selectively [49]. The sensors with coated wire are frequently composed of high conductivity metal wire, such as precious metals, copper, and aluminum. The active sites are distributed on a polymer matrix covering the top of a substrate of metal wire. Although further studies are needed to achieve adequate analyte selectivity, chemical metal oxide sensors have been shown to be reliable in the detection of reducing gasses. They provide a cost-effective sensing option for medical devices, industrial and domestic ventilation control, and other approaches [50].

The synthetic opioid agonist-antagonist nalbuphine HCl has a molecular structure with both the opioid antagonist naloxone and the powerful opioid agonist oxymorphone. Compared to other opioid analgesics, nalbuphine is used primarily in hospitals and is rarely recommended by physicians as an injectable formulation [51,52]. In addition, nalbuphine's strong antagonistic effects make it less attractive as a substitution agent for heroin addicts or opioid users with high tolerance [53]. According to some anecdotal reports, nalbuphine is abused by health professionals and bodybuilders [54].

The basic methods for the determination of NBP are chemiluminescence [55], spectrofluorimetry [56], chromatographic separation [57], and electrochemical methods [58]. These methods are considered very expensive because they require the use of an extraction solvent. In addition, highly skilled personnel are required due to the complexity of these methods. Electrochemical probs are rapid techniques, more efficient and less expensive for a diversity of analytical determinations [59]. Although several approaches have been reported for the determination of NBP, no biogenically modified metal oxide sensors for the determination of NBP have been reported to date. Therefore, the main objective of this study is to utilize *Salvia officinalis* leaf extracts to prepare two nanocatalysts, alumina and copper oxide nanoparticles. The prepared nanomaterials were characterized. The catalytic efficacy of the biogenically prepared metal oxides to improve the potential of sensing systems was investigated using two potential sensing systems for the detection of NBP in bulk and commercial injections. The sensitivity and applicability of the developed sensor systems were evaluated by method validation according to the recommendations of the International Council of Harmonization (ICH) [60].

2. Materials and methods

2.1. Reagents and solvents

Several pure-grade chemicals were supplied from Sigma-Aldrich (Hamburg, Germany). These materials such as 37% hydrochloric acid (HCl), 97.0% tetrahydrofuran (THF), polyvinyl chloride (PVC, 99.0%), aluminum nitrate nonahydrate ($Al(NO_3)_3$. $9H_2O$, 99.00%), phosphomolybdic acid (PMA, 99.99%), copper nitrate trihydrate ($Cu(NO_3)_2$. $3H_2O$), and solvents including acetone, ethanol and methanol with high purity 99.0%. Pure nalbuphine was kindly gifted by Amoun Pharmaceuticals Co. (Cairo, Egypt), and Nalufin® 20 mg/1 mL was obtained from local pharmacies (Cairo, Egypt).

2.2. Preparation of plant extract

Salvia officinalis (sage) leaves were cleaned and dried, then pulverized and extracted by boiling the dried leaf powder (10 g) in Milli-Q water (500 mL) at 100 °C for 30 min. The extract was filtered using Fisherbrand™ grade 55 filter paper with a pore size of 3 μm once it had cooled to room temperature. The extracted material was used to prepare metal oxide nanoparticles (Scheme 1a).

2.3. Biogenic preparation of nanomaterials

The co-precipitation method is the simultaneous precipitation of several compounds from a solution. It is the most practical method for the preparation of nanoparticles, in which a metal precipitates as a hydroxide from a salt precursor in the presence of a base in a solvent [61]. The synthesis of Al_2O_3NPs and CuONPs was conducted using Sage plant extract. The synthesis process was usually carried out by separately mixing 50 mL of copper nitrate trihydrate (1.0 mol L^{-1}) or aluminum nitrate nonahydrate (1.0 mol L^{-1}) in Milli-Q water and 100 mL of *Salvia officinalis* leaf extract which contains several bioactive components, including phenolic acids, terpenoids, and flavonoids. These phytoconstituents reduce and stabilize the nanoparticles during the preparation process, give the necessary flexibility for excellent control of nanomaterials size and shape. The mixture was heated at 80 °C for 30 min with constant agitation. A few drops of sodium hydroxide (1.0 mol L^{-1}) were added dropwise for 30 min. The precipitates formed were centrifuged at 2500 rpm for 5 min and then filtered using grade 55 Fisherbrand™ filter paper with a pore size of 3 μm. The precipitates were rinsed separately with deionized water to eliminate excess sodium hydroxide. They were then air-dried (60 °C, 12 h). The dried Al_2O_3NPs and CuONPs were grinding in a mortar to prevent any agglomeration and collected and stored in tight, clean containers for further studies (Scheme 1b). The chemical equations (1)–(4) for the preparation of Al_2O_3NPs and CuONPs were presented as follow:

$$Al\ (NO_3)_3 + 3NaOH \rightarrow Al(OH)_3 + 3NaNO3 \quad (1)$$

$$2Al(OH)_3 \rightarrow Al_2O_3 + 3H_2O \quad (2)$$

$$Cu(NO_3)_2 + 2NaOH \rightarrow Cu(OH)_2 + 2NaNO3 \quad (3)$$

$$2Cu(OH)_2 \rightarrow 2CuO + 2H_2O \quad (4)$$

2.4. Characterizations

To characterize and confirm the synthesis of Al_2O_3NPs and CuONPs, several analytical techniques were used, such as Fourier transform infrared spectroscopy (FT-IR, PerkinElmer, Massachusetts, USA). X-ray diffraction (XRD, Shimadzu diffractometer, XRD-6000, Kyoto, Japan). The surface morphology and size of the formed nanoparticles and their size distribution were investigated using a JEOL-SEM, Tokyo, Japan) and a light scattering analyzer. The elemental confirmation was revealed using energy dispersive X-ray (EDX).

2.5. Preparation of NBP authentic solution

Each day, 0.357 g of NBP was dissolved in 100 mL of Milli-Q water to obtain an authentic NBP solution of 1.0×10^{-2} mol L^{-1}. The Milli-Q water was used to prepare serial dilution of NBP solutions for subsequent measurements.

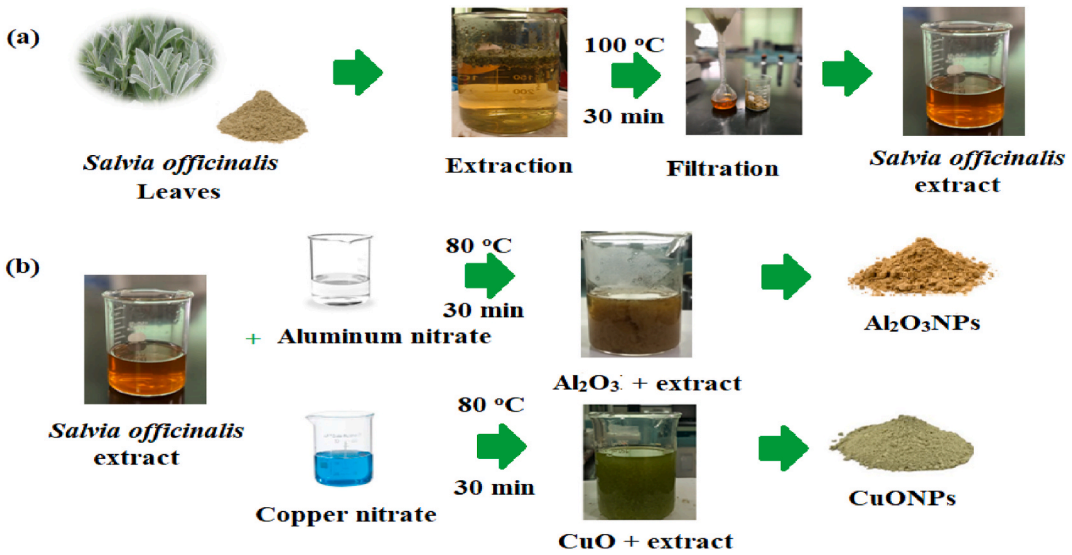

Scheme 1. Biogenic synthesis of metal oxide nanoparticles (a) extraction steps of *Salvia officinalis* leaves and (b) Synthesis of Al_2O_3NPs and CuONPs using *Salvia officinalis* leaves extract.

2.6. Formation of ion-pair material

The ion-pair material of NBP-PM was obtained by interacting 50 mL of the selected drug (NBP, 1.0×10^{-2} mol L^{-1}) with a similar volume of phosphomolybdic acid (PMA, 1.0×10^{-2} mol L^{-1}). A greenish-yellow precipitate was formed from NBP-PM, which was filtered using grade 55 Fisherbrand™ filter paper with a pore size of 3 μm. The precipitate was baked overnight at room temperature [62]. Ex-situ method was used to anchor the formed electroactive NBP-PM material with metal oxide nanoparticles. This process was conducted by dispensing (5 mg) of previously prepared Al_2O_3NPs or CuONPs in 190 mg of polyvinyl chloride polymer solution using solvent mediator THF (5 mL). This method of preparation is commonly used because it has not any limitations on the nature and physicochemical properties of nanoparticles and host polymer [63].

2.7. Membrane formation and sensor design

Three designed NBP-PM, NBP-PM-Al_2O_3NPs, and NBP-PM-CuONPs were prepared by mixing 190 mg (PVC), 10 mg active complex (NBP-PM), and 0.35 mL fluidizing agent *o*-NPOE in 5 mL THF [64]. The wire of each sensor was then polished and cleaned with acetone. The standard sensor NBP-PM was prepared by continuously immersing an Al wire in the membrane matrix. To obtain the functionalized sensors, a membrane matrix possessing Al_2O_3NPs or CuONPs (5 mg), PVC (190 mg), NBP-PM active complex (10 mg), and *o*-NPOE fluidizing agent (0.35 mL) was suspended in 5 mL THF. Nalbuphine, which is derived chemically from oxymorphone, is a powerful analgesic with narcotic antagonist effect. Due to the scarcity of methamphetamine, the misuse of nalbuphine as a substitute for methamphetamine has increased [65]. Accordingly, analytical approaches for NBP detection may be of interest, particularly in settings when traditional techniques are ineffective, as is the case in many on-site tests and fast screening applications. In these sectors, potentiometric sensing devices, such as analyte selecting sensors, play an essential role.

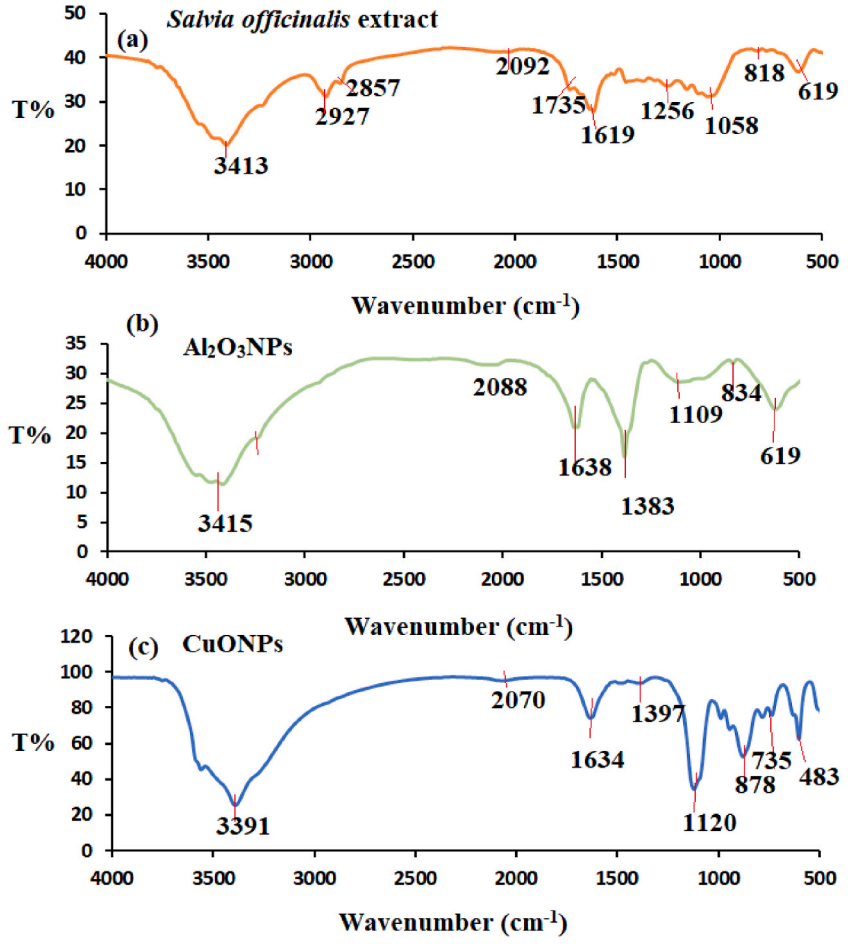

Fig. 1. Functional groups analysis of (a) Sage extract, (b) Al_2O_3NPs, and (c) CuONPs by Sage extract.

2.8. Regression equations and calibration plots

To estimate the regression equations and to construct the calibration plots for the developed NBP sensors, approximately 50 mL of a 1.0×10^{-9}-1.0×10^{-2} mol L^{-1} NBP solution was individually measured. Calibration plots were created by plotting potential values against the -logarithm of NBP concentrations.

2.9. Adjustment of the measurement conditions

Independent pH is one of the influencing factors that should be investigated and adjusted. The influence of different pH values from 1 to 9 with 1.0×10^{-3} mol L^{-1} of NBP solution was used. A pH glass electrode and the indicated potentiometric device was applied. The pH was optimized a few drops of 0.1 mol L^{-1} hydrochloric acid or sodium hydroxide. The pH graph was then constructed [64].

As is common in such studies, the selectivity of NBP-sensors was evaluated using a separate solution approach [64]. The estimated tolerable results for a number of interfering components, including potential cations (K^+, Mg^{2+}, Al^{3+}, Ca^{2+}, Zn^{2+}, and Na^+), sugars, and amino acids were performed. The estimated values of K_{pot} were evaluated using separate solution method and calculated using equation (5) used by Rana et al. [64].

$$\text{Log } K_{pot} = (E2 - E1) \Big/ S + \log[\text{Drug}] - \text{Log } [B^{z+}]^{1/z} \quad (5)$$

where these values represent selectivity coefficient (Kpot), sensor response of 1.0×10^{-3} mol L^{-1} NBP (E1), sensor response of 1.0×10^{-3} mol L^{-1} of interfering species, B^{z+} (interferingspecies), and slope of the linear plot (S), respectively.

The response time of NBP modified sensors was evaluated for NBP of 1.0×10^{-9} to 1.0×10^{-2} mol L^{-1} solutions.

2.10. Assay of NBP in Nalufin®20 mg/1 mL ampoule

The contents of 20 NBP ampoules containing 0.4 g NBP were diluted to 100 mL with Milli-Q water to gain an NBP standard solution with a concentration of 1.0×10^{-2} mol L^{-1}. Further dilutions with the same solvent were made to obtain NBP samples with a concentration of 1.0×10^{-9}-1.0×10^{-2} mol L^{-1}. The designed NBP-PM, NBP-PM-Al_2O_3NPs and NBP-PM-CuONPs sensors were used separately to determine the studied samples.

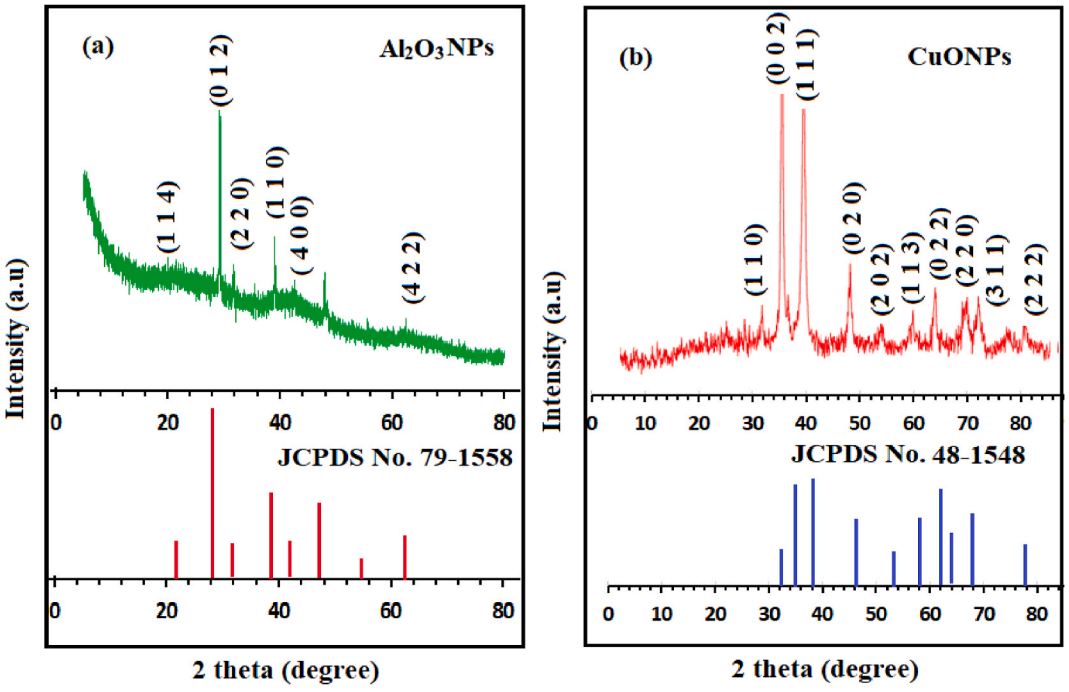

Fig. 2. XRD spectra of (a) Al_2O_3NPs (Reference card No. 79–1558) and (b) CuONPs (Reference No.48-1548) synthesized by Sage extract.

3. Results and discussion

3.1. Identification of the synthesized nanoparticles

The synthesized Al_2O_3NPs and CuONPs using the extract of sage leaves were characterized by various analytical techniques. Fig. 1a shows the FT-IR spectra of a *Salvia officinalis* (sage) leaves extract. The functional groups of polyphenols O–H (3413 cm^{-1}), methyl groups C–H (2927 and 2857 cm^{-1}), carbonyl group within aromatic ring of flavonoids and polyphenols C═O (2092 cm^{-1}), alkene C═C (1735 cm^{-1}) and strong ester C–O (1619, 1256, and 1058 cm^{-1}), respectively. C-halo compound (818-619 cm^{-1}) were observed. These findings are matched those addressed in the literature [66].

For FT-IR spectrum of Al_2O_3NPs (Fig. 1b) shows various absorption bands at 3391, 2070, 1634, 1397, 1120, 878, 737, and 483 cm^{-1} attributed to strong O–H stretching vibration of phenolic compounds, strong S–C≡N stretching of isothiocyanate, C═C vibration of monosubstituted alkene, medium O–H bending of carboxylic acid, strong C–O stretching of secondary alcohol, strong C–H bending trisubstituted, strong C–H bending monosubstituted, and Al–O stretching vibration, respectively [67].

CuONPs have several remarkable absorption bands as shown in (Fig. 1c). The related bands to the functional groups can be summarized as follows:

The functional groups of Cu–O, H–*O*–H, –OH, O–C═O, C–O, and C-halide are expressed by the stretching vibration bands at 484, 1634, 3391, 1397, 1120, 878 cm^{-1}, respectively. These results are in agreement with those reported in the literature [68].

XRD technique is used to study the crystalline structure in the materials. The XRD spectrum of Al_2O_3NPs (Fig. 2a) shows significant peaks at 2θ = 22.9° (1 1 4), 29.4° (0 1 2), 31.9° (2 2 0), 39.0° (1 1 0), 55.6° (4 2 2), 64.9° (4 4 0) crystalline planes, respectively. the results similar to (JCPDS Card No. 79–1558) [69].

The XRD determination of synthesized CuO NPs using *Salvia officinalis* leaves extract was performed for confirming their crystalline structure (Fig. 2b). Various diffraction peaks at 2θ of 32.61° (1 1 0), 35.64° (0 0 2), 38.97° (1 1 1), 48.93° (0 2 0), 53.55° (2 0 2), 58.35° (1 1 3), 61.08°(0 2 2), 66.27° (3 1 1), and 79.27° (2 2 2) were matched the standard (JCPDS No. 48–1548) which showed the monoclinical spherical crystalline nature. The following equation (6) was applied to evaluate the grain size of nanomaterials [70].

$$D = 0.95\lambda/\beta \cos\theta \tag{6}$$

where these values represent (particle size, D nm), (constant, K = 0.95), (wavelength $\lambda = 1.54 \times 10^{-10}$), (FWHM, B), and (Bragg angle degree, θ), respectively. Thus, average grain size of green synthesized of Al_2O_3NPs and CuO NPs was found as 18.8 ± 1.4 nm for both metal oxides.

The morphological surface of the synthesized Al_2O_3NPs and CuONPs was investigated using SEM. The appearance and shape of the produced metal oxides were identified at 30,000x and 50,000× magnifications. Fig. 3a and b shows SEM images of Al_2O_3NPs and CuONPs. They exhibited largely polydisperse, spherical particles, but all were interconnected or closely related. The size of the particles was 55.07 ± 4.15 and 59.48 ± 4.50 nm, for Al_2O_3NPs and CuONPs. The tiny particles were so close together that they appeared to be embedded in the surface. The only structures or morphologies seen in the generated samples were Al_2O_3NPs and CuONPs.

The nanosized distribution was also measured by DLS, and the mean Al_2O_3NPs and CuONPs sizes were found around 40–60 nm, respectively (Fig. 4a and b).

The elemental determination of the prepared nanostructured (Al_2O_3NPs and CuONPs) was investigated using an EDX spectroscopy.

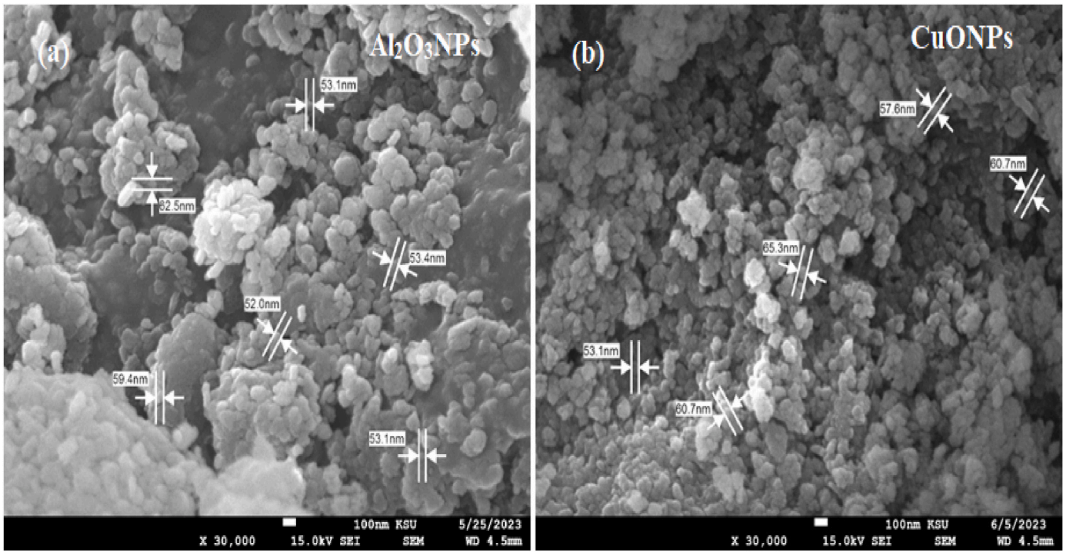

Fig. 3. Scanning electron microscope (SEM (a) Al_2O_3NPs & (b) CuONPs forming by Sage extract.

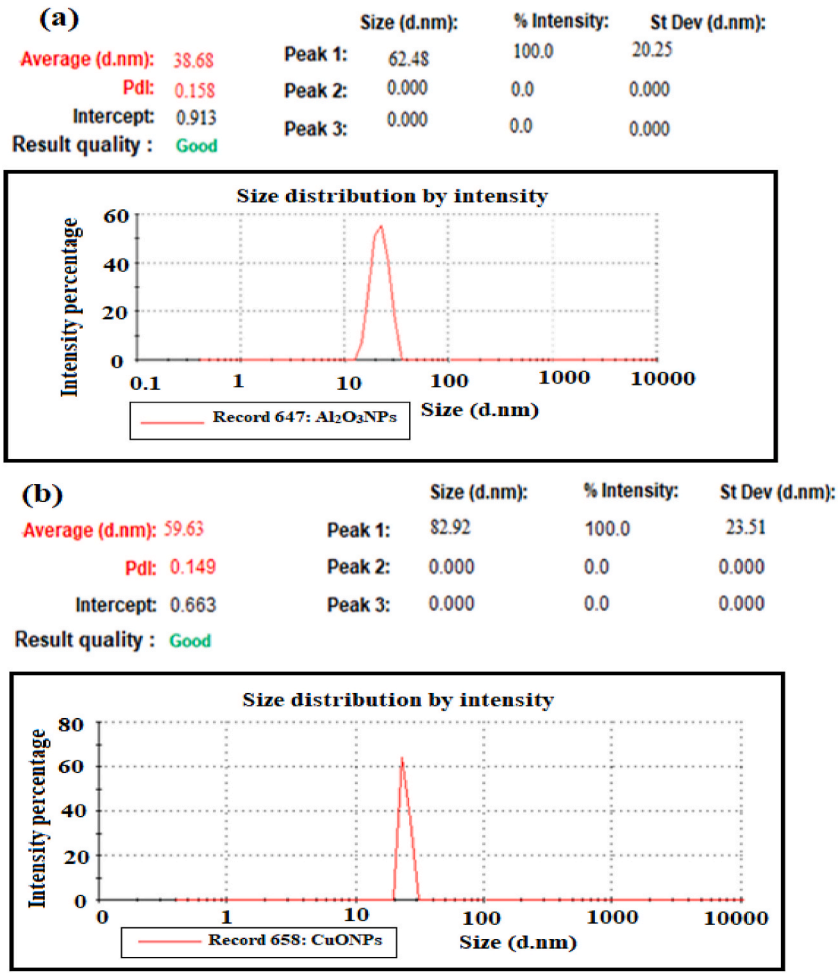

Fig. 4. DLS of biogenically formed (a) Al_2O_3NPs & (b) CuONPs using Sage extract.

The w% of Al and O is 32.59% for Al and 67.41% for O, whereas A% of Al is 22.18% and of O is 77.72%. However, the CuONPs sample shows 47.49% Cu and 52.51% O, with a Cu atomic percentage of 34.11% and an O atomic percentage of 65.89% (Fig. 5a and b).

The elemental mapping of the pre-synthesized Al_2O_3NPs and CuONPs showed the presence of pure metal oxide nanoparticles (Fig. 6a and b)

3.2. Nalbuphine-sensors behavior

The reaction of NBP with PM produces the stable active complex NBP-PM, which is soluble in THF. The active components were added to both standard and functionalized NBP sensors, with fluidizing agent serving as the dissolving medium in the existence of polymeric matrix. The main properties of the proposed NBP-sensors were presented in Table 1. The recorded data indicated that the potential responses of the three designed potentiometric systems were (53.9 ± 0.6 mV, 1.0×10^{-6}-1.0×10^{-2} mol L^{-1}), (56.143 ± 0.4 mV, 1.0×10^{-8}-1.0×10^{-2} mol L^{-1}), and (58.476 ± 0.2 mV, 1.0×10^{-9}-1.0×10^{-2} mol L^{-1}), respectively. Scheme 2 shows a possible pathway for drug sensor interaction (Fig. 7).

The clean aluminum wire was coated with an electroactive mixture, resulting in various potential spots on the exterior part of sensor. The inclusion of nanoscale metal oxides with different physicochemical features, such as Al_2O_3NPs and CuONPs, in the membrane composition elevated the conduction of active spots owing to its high dielectric permittivity, high conductivity, mechanical and chemical stability, and large surface area, which enhance the NBP^+ in the sample and the potential spots distributed on the membrane superficial.

3.3. Response and soaking time

The response time of the prepared sensors were constant after 60, 45, 40 s over the tested concentration, respectively. The reproducibility of the proposed sensors during their lifetime was explored, and the results gave good reproducibility. The sensors have

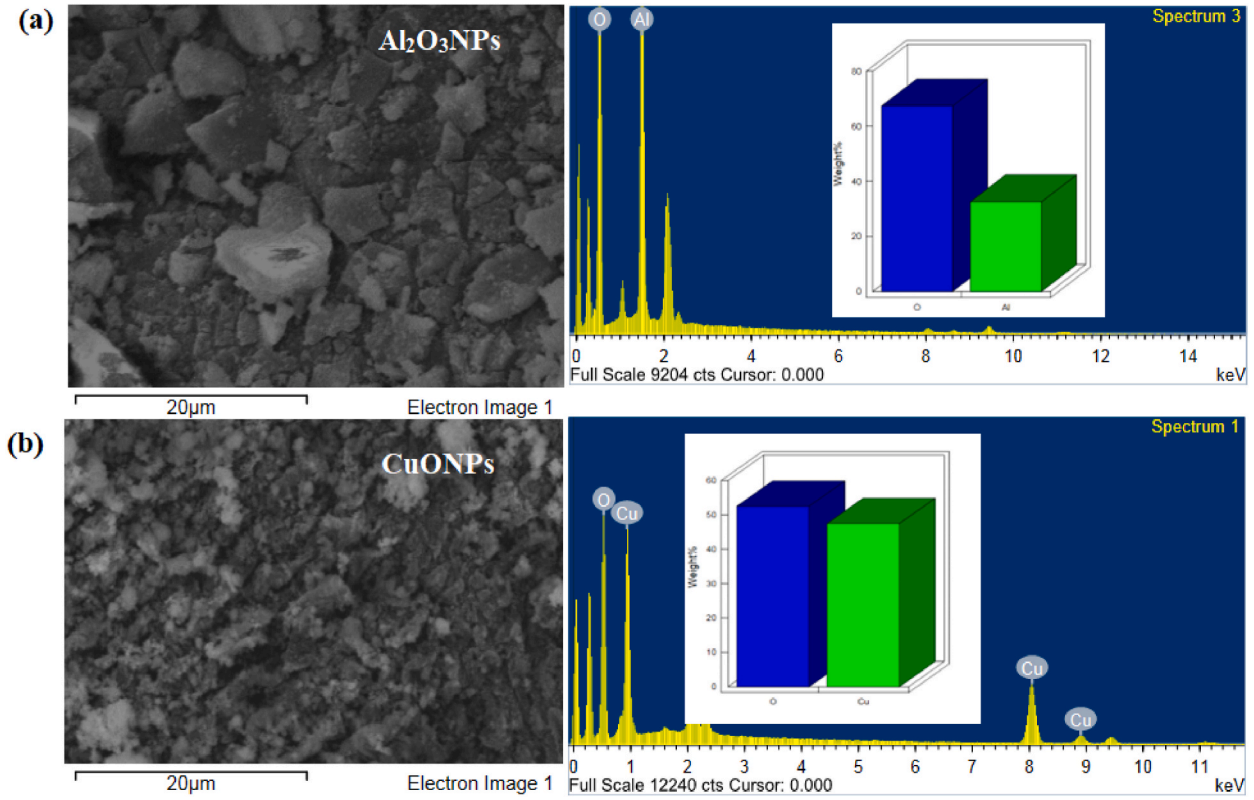

Fig. 5. EDX spectra of biogenically synthesized (a) Al_2O_3NPs and (b) CuONPs using leaves extract of *Salvia officinalis* (sage).

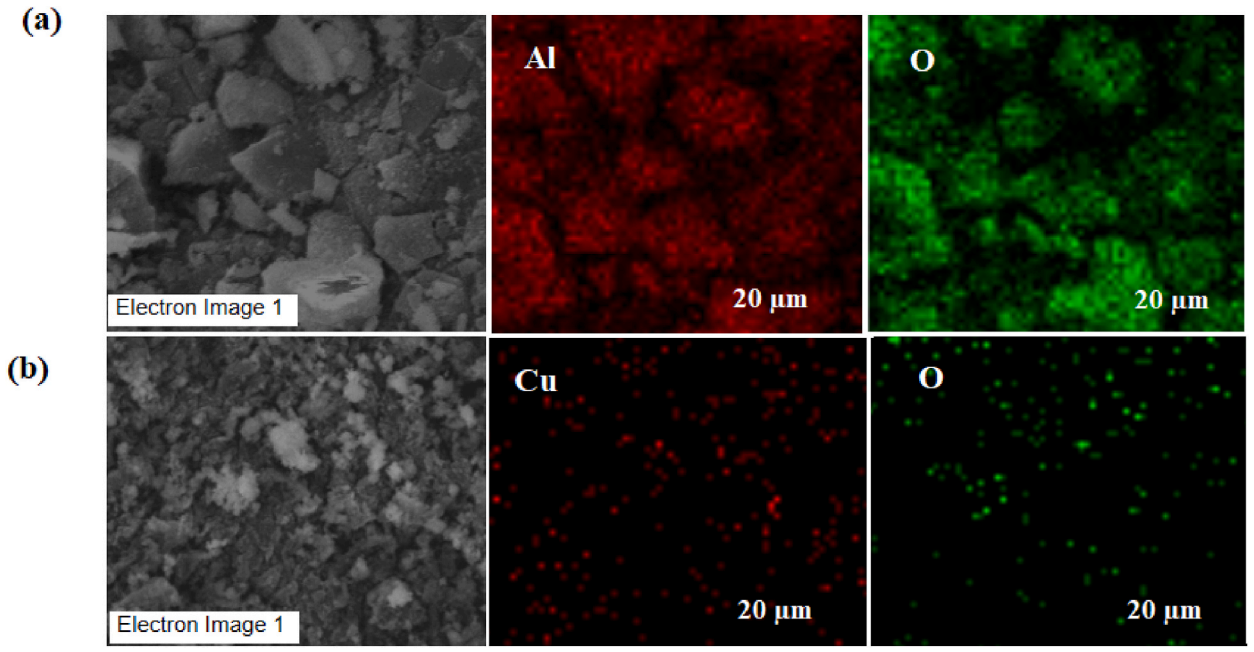

Fig. 6. Mapping of biogenically synthesized (a) Al_2O_3NPs and (b) CuONPs using Sage leaves extract.

Table 1
The potential characteristics of NBP-sensors for the assay of NBP samples.

Parameters	NBP-PM sensor	NBP-PM-Al_2O_3NPs sensor	NBP-PM-CuONPs sensor
Linear range (M)	1.0×10^{-6} -1.0×10^{-2}	1.0×10^{-8} -1.0×10^{-2}	1.0×10^{-9} -1.0×10^{-2}
Regression equation r, (correlation coefficient)	$E_{mV} = (53.9 \pm 0.6)$ log (NBP) + 421.6	$E_{mV} = (56.143 \pm 0.4)$ log (NBP) +607.86	$E_{mV} = (58.476 \pm 0.2)$ log (NBP) + 724.8
S_a uncertainty of intercept	0.9996	0.9999	0.9999
S_b uncertainty of slope	3.6249	1.14107	1.83782
Working pH range	0.8544	0.21189	0.308454
Temperature, °C	3–8	3–8	3–8
Response time/s	25	25	25
Lifetime/day	60	45	40
Accuracy (%)	30	50	60
Lower detection limit (M)	98.79 ± 0.64 5.0×10^{-7}	99.28 ± 0.58 4.8×10^{-9}	99.52 ± 0.28 5.0×10^{-10}

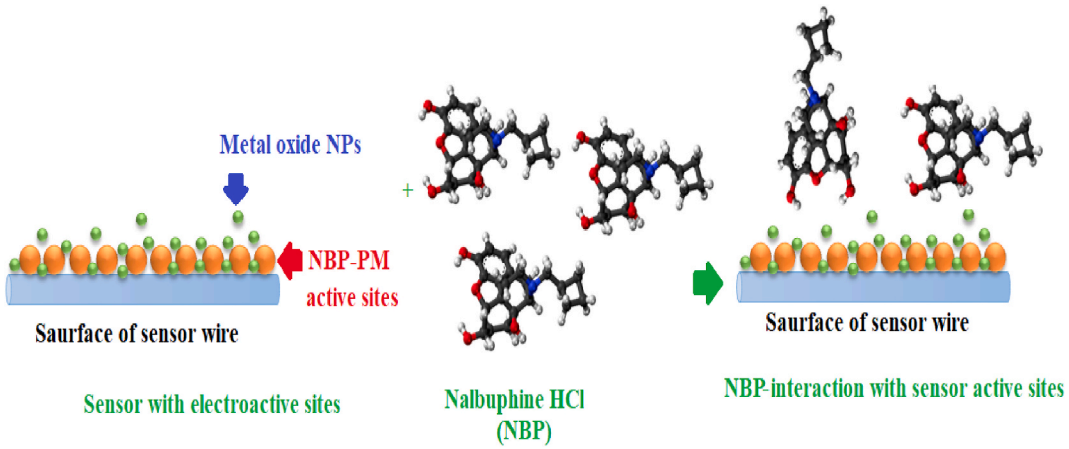

Scheme 2. Schematic representation of the interaction between NBP and active sites on the sensor surface.

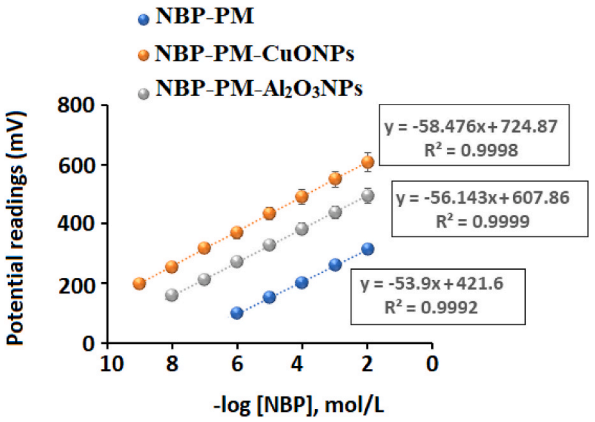

Fig. 7. Linear regression equations of (a) NBP-PM, (b) NBP-PM-CuONPs, and (c) NBP-PM-Al_2O_3NPs using 1.0×10^{-9}-1.0×10^{-2} mol L^{-1} NBP authentic samples.

lifetimes of 30, 50, and 60 days, during and their slopes remained constant with good repeatability. The impact of soaking times on the probable activities of NBP-sensors was explored by immersing the designed sensors for 1–6 h, and overnight. It was observed that the suitable conditioning time was 4 h for the three constructed membranes.

3.4. Effect of plasticizers

As is widely known, the final potentiometric readings of sensors in terms of stability and selectivity, etc. is determined not only by

the electroactive materials, but also by the employment of a specific plasticizer and the amount of the various membrane constituents. Because of the number of these parameters, multiple proportions of the membrane components (ion-pair, plasticizer, and PVC) were evaluated in the first stage. Because of the number of these parameters, different proportions of the membrane components (ion-pair, plasticizer, and PVC) were evaluated in the first stage. In addition, three plasticizers were used to fabricate distinct membranes: dibutyl sebacate (DBS), dioctyl phthalate (DOP), and *o*-nitrophenyl octyl ether (*o*-NPOE). Fluidizing agents induce a remarkable effect on membrane qualities by acting as a fluidizer and allowing the membrane's material to disintegrate completely. Table 2 shows the potential behavior of the developed sensors utilizing various plasticizers.

The outcomes indicated that the potential responses of NBP-PM (Sensor 1) in the presence of different plasticizers DBS, DOP, and *o*-NPOE were 48, 50, and 52 mV decade^{-1}, respectively. However, the modified NBP-PM-Al_2O_3NPs (Sensor 2) shows potential responses 52, 53, and 55 for the same plasticizers, respectively. Whereas for sensor 3 excellent potential responses 55, 56, and 58 were observed. These results can be ascribed to the fact that the ε value of (DBS, $\varepsilon = 4.5$), (DOP, $\varepsilon = 5.1$), and (*o*-NPOE, $\varepsilon = 24$). Therefore, the use of *o*-NPOE shows excellent potential responses for the three designed sensors.

3.5. pH investigation

To determine the suitable pH values for NBP detection, the potential of the standard and metal oxide functionalized sensors were examined with respect to several pH values (Fig. 8). The results show that all designed NBP-PM, NBP-PM-CuONPs, and NBP-PM-Al_2O_3NPs sensors are essentially ineffective in the pH range 3–8. Whereas at pH above 8, a progressive reduction in response values was noticed, which might be due to the struggle of NBP^+ and the hydroxyl ions of sodium hydroxide in the testing sample [71].

3.6. Interferences

The designed sensors were evaluated for the measurement of 1.0×10^{-3} M of several foreign materials to examine the discernment of the developed NBP sensors for the studied drugs. As a result, the functionalized sensors NBP-PM-Al_2O_3NPs and NBP-PM-CuONPs showed exceptionally good selectivity. The addition of Al_2O_3NPs and CuONPs boosts the conduction property of the developed sensors as well as enhancing the detectability of the testing sample due to difference in the physicochemical properties and grain size of the synthesized nanoparticles. The developed method showed no effect of the interferent ions on the quantification of NBP (Table 3)

3.7. Assay of nalbuphine hydrochloride in authentic samples

Percent recoveries of NBP in authentic samples were determined using the three NBP-sensors. The resulting values were 98.79 ± 0.64%, 99.28 ± 0.58%, and 99.52 ± 0.28, respectively (Table 4).

The higher efficiency of sensor was related to the chemical stability and physical features of added nanomaterials. Moreover, since CuONPs have higher dielectric constant than Al_2O_3NPs, the sensor functionalized with CuONPs showed good efficiency and applicability for NBP measurement.

3.8. Method validation

The described method was revealed and evaluated using the criteria of ICH [60].

The outcomes indicated that the potential responses of the three designed potentiometric systems were (53.9 ± 0.6 mV, 1.0×10^{-6}-1.0×10^{-2} mol L^{-1}), (56.143 ± 0.4 mV, 1.0×10^{-8}-1.0×10^{-2} mol L^{-1}), and (58.476 ± 0.2 mV, 1.0×10^{-9}-1.0×10^{-2} mol L^{-1}), for NBP-PM, NBP-PM-Al_2O_3NPs, and NBP-PM-CuONPs, respectively. The correlation coefficients of the NBP-sensors were determined from the least squares regression equations (Fig. 7) and were found >0.999. The uncertainty of slope (S_b, 0.8544, 0.21189, and 0.308454) and intercept (S_a, 3.6249, 1.14107, and 1.83782) for the proposed sensors were calculated from the calibration graphs of the three designed sensors using Excel program, windows 10.

To evaluate the lesser detection value, the response values of NBP-sensors were measured when the slope was dropped by the value 17.9 mV [71]. The resulting values were 5.0×10^{-7}, 7.8×10^{-9}, and 5.0×10^{-10} mol L^{-1}.

The developed approach was investigated for its accuracy by measuring 9 NBP pure solutions, and the relative % recovery ± standard deviation was calculated to be 98.79 ± 0.64%, 99.28 ± 0.58%, and 99.52 ± 0.28%, respectively, for the sensors NBP-PM, NBP-PM-Al_2O_3NPs, and NBP-PM-CuONPs (Table 4).

The precision of anticipated electrochemical systems was investigated with intra-and inter-day tests, the findings were computed calculated the (RSD%) of varying concentrations of authentic NBP samples (Table 5). The RSD% for the working systems were (0.4%, 0.3%, and 0.7%) and (0.2%, 0.6%, and 0.7%) for intra-day and (0.4%, 0.6%, and 0.3%) and (0.5%, 0.8%, and 0.4%) inter-day measurements, respectively revealing high precision of the designed NBP-PM-Al_2O_3NPs, and NBP-PM-CuONPs.

3.9. Nalbuphine hydrochloride injection assay

To evaluate the analytical application of the studied sensors, NBP was evaluated in the injection (Nalufin®20 mg/1 mL). All resulting values were compared with various NBP samples and the main recovery percent was estimated from the calibration graph. The related values for NBP sensors were 98.35 ± 0.84, 99.28 ± 0.59, and 99.59 ± 0.57 (Table 6). In the assay of NBP, it was found that the NBP-PM-CuONPs sensor exhibits high sensitivity than NBP-PM-Al_2O_3NPs sensor. The higher conductivity of the modified CuONPs

Table 2
Influence of fluidizing agent on the response of the constructed NBP sensors.

Fluidizing agent	Dibutyl sebacate	Dioctyl phthalate	*o*-NPOE
Sensor (1)	NBP-PM		
Response time	45	30	25
Slope	49	49	51
Calibration range	4.0×10^{-6}-1.0×10^{-2}	2.5×10^{-5}-1.0×10^{-2}	1.0×10^{-6}-1.0×10^{-2}
Sensor (2)	NBP-PM-Al_2O_3NPs		
Response time	30	25	20
Slope	52	53	55
Calibration range	1.0×10^{-6}-1.0×10^{-2}	9.0×10^{-6}-1.0×10^{-2}	1.0×10^{-7}-1.0×10^{-2}
Sensor (3)	NBP-PM-CuONPs		
Response time	25	30	20
Slope	55	56	58
Calibration range	1.0×10^{-7}-1.0×10^{-2}	1.0×10^{-7}-1.0×10^{-2}	1.0×10^{-8}-1.0×10^{-2}

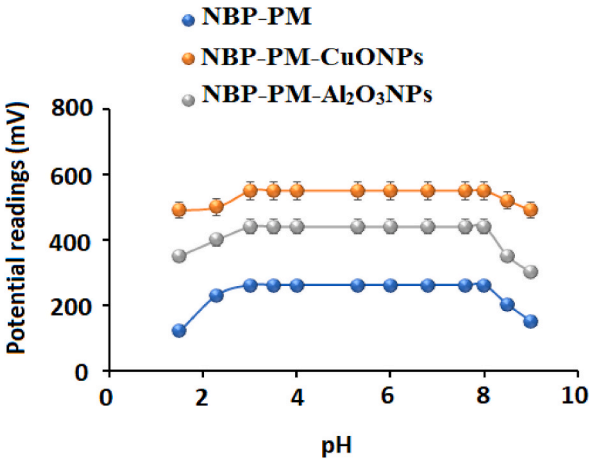

Fig. 8. pH measurement ranges for the fabricated NBP-PM, NBP-PM-CuONPs, and NBP-PM-Al_2O_3NPs using NBP authentic sample.

Table 3
The selectivity effect of the designed NBP-sensors using separate solution method.

Interferences	NBP-PM (K^{Pot} NBP)	NBP-PM-Al_2O_3NPs (K^{Pot} NBP)	NBP-PM-CuONPs (K^{Pot} NBP)
K^+	1.9×10^{-3}	2.5×10^{-4}	4.3×10^{-4}
Mg^{2+}	3.2×10^{-3}	3.7×10^{-4}	6.2×10^{-4}
Al^{3+}	4.8×10^{-3}	2.2×10^{-4}	4.7×10^{-4}
Ca^{2+}	9.1×10^{-3}	6.3×10^{-4}	5.8×10^{-4}
Zn^{2+}	3.7×10^{-3}	5.6×10^{-5}	5.3×10^{-5}
Na^+	5.8×10^{-3}	3.8×10^{-4}	4.0×10^{-4}
Sucrose	4.2×10^{-3}	1.2×10^{-4}	2.3×10^{-4}
Glucose	9.1×10^{-3}	9.8×10^{-4}	1.0×10^{-5}
Lactose	2.6×10^{-3}	3.6×10^{-4}	6.5×10^{-4}
L-histidine	1.1×10^{-3}	2.4×10^{-4}	8.7×10^{-4}
Glycine	8.7×10^{-3}	4.7×10^{-4}	6.4×10^{-4}
L-valine	4.6×10^{-3}	4.6×10^{-4}	7.8×10^{-4}
Leucine	1.9×10^{-3}	2.7×10^{-4}	3.2×10^{-4}

sensor than Al_2O_3NPs can be due to the fact that CuONPs have a higher dielectric constant ($\varepsilon = 10^4$) than Al_2O_3NPs ($\varepsilon = 8.9$). Statistical analysis was applied to assess the obtained data [72].

Table 7 compares the results acquired with the suggested NBP-sensors to those previously examined with other analytical techniques [73–80] in order to assess the advanced characteristics, and applicability of the modified NBP-nano sensors for NBP quantification. Attia et al. reported a spectroscopic method for the estimation of NBP after its oxidative stress. The developed method showed a linear concentration range of 1.0–20 μg mL^{-1} with a detection limit of 0.287 μg mL^{-1}. Another spectrophotometric technique was developed using univariate and multivariate regression methods, which successfully measured NBP at 40–80 ppm. In addition, two spectrofluorimetric and chemiluminescence methods for estimating NBP using Ce (IV) and ruthenium in acidic medium were investigated, providing drug detection at 2.4–8.4 and 0.001–15 ppm, consistently. The chromatographic separation technique was also used

Table 4
The assay of nine NBP concentrations utilizing three designed NBP-sensors for accuracy study.

Statistical data	NBP-PM sensor			NBP-PM-Al_2O_3NPs sensor			NBP-CuONPs sensor		
	[a]Sample	[a]Values	% recovery	[a]Sample	[a]Values	% recovery	[a]Sample	[a]Values	% recovery
	6.0	5.96	99.33	8.0	7.98	99.75	9.0	8.99	99.88
	5.3	5.24	98.86	7.3	7.26	99.45	8.3	8.27	99.63
	5.0	4.89	97.80	7.0	7.00	100.00	8.0	7.95	99.38
	4.3	4.25	98.84	6.3	6.25	99.21	7.0	6.96	99.43
	4.0	3.96	99.00	6.0	5.97	99.50	6.0	5.98	99.67
	3.3	3.25	98.00	5.0	4.99	99.80	5.0	4.99	99.80
	3.0	2.94	99.50	4.0	3.94	98.50	4.0	3.97	99.25
	2.3	2.26	98.26	3.0	2.95	98.33	3.0	2.99	99.67
	2.0	1.99	99.50	2.0	1.98	99.00	2.0	1.97	99.00
Mean ± SD n	98.79 ± 0.64			99.28 ± 0.58			99.52 ± 0.28		
Variance	9			9			9		
%SE	0.41			0.34			0.08		
%RSD	0.21			0.19			0.09		
	0.65			0.58			0.28		

[a] Sample and values = -log [NBP], (M).

Table 5
Precision results of NBP-sensors using three authentic samples of NBP.

Investigated sensor	Type of measurement	Sample (M)	% recovery[a]	%RSD	%Er**
NBP-PM-Al_2O_3NPs	Intra-day precision	8.0	99.35 ± 0.4	0.4	0.23
		6.0	98.78 ± 0.3	0.3	0.17
		2.0	99.16 ± 0.7	0.7	0.40
	Inter-day precision	8.0	98.89 ± 0.4	0.4	0.23
		6.0	99.64 ± 0.6	0.6	0.35
		2.0	98.58 ± 0.3	0.3	0.17
NBP-PM-CuONPs	Intra-day precision	9.0	99.78 ± 0.2	0.2	0.11
		6.0	99.13 ± 0.6	0.6	0.35
		3.0	98.87 ± 0.7	0.7	0.40
	Inter-day precision	9.0	99.63 ± 0.5	0.5	0.29
		6.0	99.37 ± 0.8	0.8	0.46
		3.0	99.43 ± 0.4	0.4	0.23

[a] n = 3 measurements ** % Er= SD/$\sqrt{n}$.

Table 6
Assay of NBP in various analytical samples of Nalufin® 20 mg/1 mL using NBP-sensors.

Statistical data	NBP-PM sensor			NBP-PM-Al_2O_3NPs sensor			NBP-CuONPs sensor		
	*Taken	*Outcome	% recovery	*Taken	*Outcome	% recovery	*Taken	*Outcome	% recovery
	6.0	5.95	99.17	8.0	7.98	99.75	9.0	8.99	99.89
	5.3	5.24	98.87	6.0	5.96	99.33	8.0	7.96	99.50
	5.0	4.89	97.80	5.0	4.95	99.00	7.0	7.00	100.00
	4.0	3.93	98.25	4.0	3.97	99.25	6.0	5.98	99.67
	3.0	2.97	99.00	3.0	2.95	98.33	5.0	5.00	100.00
	2.0	1.99	99.50	2.0	2.00	100.00	2.0	1.97	98.50
Mean ± SD n	98.77 ± 0.63			99.28 ± 0.59			99.59 ± 0.57		
%RSD	6			6			6		
%SE**	0.64			0.58			0.57		
Variance t-student test	0.26			0.24			0.23		
F-test	0.39			0.34			0.32		
	1.705 (2.228) ***			0.459 (2.228) ***			0.337 (2.228)***		
	1.22 (5.05) ***			1.71(5.05) ***			1.81(5.05)***		
Reference	99.46 ± 0.76								
Technique [73]	6								
	0.76								
	0.31								
	0.58								

*-log [NBP], M **SE = $\sqrt{SD}/n$ *** tabulated t and F values at $p= 0.05$ [72].

for the determination of NBP using the mobile phase sodium acetate and acetonitrile. The obtained results showed acceptable quantification of NBP at 1–15 ppm. In addition, some electrochemical probs have described for the assay of NBP with rectilinear values of 0.6–10.0 μM, 0.04–850 μM, and 2.4×10^{-7}- 5.0×10^{-2} mol L^{-1}. According to the results, the recently created nano-NBP sensors

Table 7
Outcomes from the assay of NBP-sensors with previously reported analytical techniques.

Method of analysis	Chemicals and reagents	Linear range	LOD	Reference
Spectrophotometry	Oxidative stress assay	1.0–20 ppm	0.287 ppm	[73]
	Univariate and multivariate regression methods	40–80 ppm	–	[74]
Spectrofluorimetry	Oxidation using Ce (IV)	2.4–8.4 ppm	0.0142 ppm	[75]
Chemiluminescence	Acidic ruthenium (II) chloride	0.001–15 ppm	0.0005 ppm	[76]
Chromatographic separation	Sodium acetate and acetonitrile	1.0–15 ppm	0.243 ppm	[77]
Electrochemical	Nano Cobalt oxide modified sensor	0.6–10 μM	0.58 *n* M	[78]
	Pt–Pb-doped NiO modified carbon nanotubes	0.04–850 μM	0.9 *n* M	[79]
	Carboxylated multi-walled carbon nanotubes-polyaniline and polyvinyl chloride	$2.4 \times 10^{-7} - 5.0 \times 10^{-2}$ M	1.1×10^{-7} M	[80]
Current study	Sensors-based biogenically synthesized metal oxide nanoparticles	1.0×10^{-8}-1.0×10^{-2} M	4.8×10^{-9} M	NBP-PM-Al_2O_3NPs
		1.0×10^{-9} -1.0×10^{-2} M	5.0×10^{-10} M	NBP-PM-CuONPs

have better efficiency and detect minimum drug concentration than earlier approaches. These results can be attributed to the fact that metal oxide nanomaterials exhibit exceptional and improved physicochemical and mechanical properties compared to their solid counterparts. These properties can be attributed to their excellent specific and large surface extent. In general, the high surface extent of nanomaterials increases as the size of nanoparticles decreases. Moreover, the reduction in size of the materials leads to quantum confinement phenomena that change their inherent properties compared to comparable bulk materials [81]. Therefore, the use of Al_2O_3 and CuONPs with dielectric constant ($\varepsilon = 9.8$ and $\varepsilon = 10^4$) improved the conductivity between the sensing materials of the modified coated wire sensor and NBP ions.

4. Conclusion

The uniqueness of the work is to design functionalized nanomaterials-based chemical sensors for nalbuphine with excellent efficiency for detection of NBP in injections. To increase the suitability of the developed NBP-sensor, the usage of modified metal oxide nanosized in its design was recommended. Green synthetic nanoparticles were promoted for sensor fabrication to improve their potential response. The integration of Al_2O_3NPs or CuONPs with the ion-pairing materials in the polymer substrate would significantly increase the quantification of the target drug with the modified sensors. Excellent results were obtained, and the developed nalbuphine sensors exhibited high efficiency and discrimination for the assay of the target analyte. The newly developed sensors showed excellent responses compared to the current conventional types. Consequently, functionalized membrane sensors with nanomaterials can be used for systematic detection of NBP.

Author contribution statement

Seham S Alterary: Conceived and designed the experiments; Performed the experiments; Analyzed and interpreted the data; Contributed reagents, materials, analysis tools or data; Wrote the paper.

Data availability statement

All data of this study have been included within the text.
Declaration of interest's statement:
The authors declare no conflict of interest.

Funding

This research was funded by the Researchers Supporting Project in King Saud University, which supported this project, and the code number is (RSP-2023/195).

Declaration of competing interest

The authors declare that they have no known competing financial interests or personal relationships that could have appeared to influence the work reported in this paper.

References

[1] N. Shahcheraghi, H. Golchin, Z. Sadri, Y. Tabari, F. Borhanifar, S. Makani, Nanobiotechnology, an applicable approach for sustainable future, 3 Biotech 12 (2022) 65, https://doi.org/10.1007/s13205-021-03108-9.

[2] M.H. Ashery, M. Elnouby, E.M. EL-Maghraby, E.M. Elsehly, Structural control of V_2O_5 nanoparticles via a thermal decomposition method for prospective photocatalytic applications, Beni-Suef Univ. J. Basic Appl. Sci. 12 (2023) 1–15, https://doi.org/10.1186/s43088-023-00350-3.

[3] J. Zander, M. Weiss, R. Marschall, Fast and facile microwave synthesis of cubic $CuFe_2O_4$ nanoparticles for electrochemical CO_2 reduction, Adv, Energy Sustain. Res. 4 (2023), 2200184, https://doi.org/10.1002/aesr.202200184.

[4] S.A. Leau, C. Lete, S. Lupu, Nanocomposite materials based on metal nanoparticles for the electrochemical sensing of neurotransmitters, Chemosensors 11 (2023) 179, https://doi.org/10.3390/chemosensors11030179.

[5] X. Ren, Y. Du, X. Qu, Y. Li, L. Yin, K. Shen, J. Zhang, Y. Liu, Controllable synthesis of ZnO nanoparticles with improved photocatalytic performance for the degradation of rhodamine B under ultraviolet light irradiation, Molecules 28 (2023) 5135, https://doi.org/10.3390/molecules28135135.

[6] C. Zhang, Y. Zhang, J. Liu, Y. Ye, Q. Chen, C. Liang, Laser irradiation synthesized carbon encapsulating ultrafine transition metal nanoparticles for highly efficient oxygen evolution, J. Electroanal. Chem. 928 (2023), 117007, https://doi.org/10.1016/j.jelechem.2022.117007.

[7] T. Hu, P. Li, W. Zhang, Y. Ye, J. Liu, Y. Cai, G. Zhang, K. Dai, C. Liang, Laser irradiation induced platinum-based bimetallic alloy nanoparticles in liquids for electrocatalytic hydrogen production, J. Alloys Compd. 934 (2023), 167914, https://doi.org/10.1016/j.jallcom.2022.167914.

[8] U.T. Khatoon, A. Velidandi, G.N. Rao, Copper oxide nanoparticles: synthesis via chemical reduction, characterization, antibacterial activity, and possible mechanism involved, Inorg. Chem. Commun. 149 (2023), 110372, https://doi.org/10.1016/j.inoche.2022.110372.

[9] V. Harish, M.M. Ansari, D. Tewari, A.B. Yadav, N. Sharma, S. Bawarig, M.L. García-Betancourt, A. Karatutlu, M. Bechelany, A. Barhoum, Cutting-edge advances in tailoring size, shape, and functionality of nanoparticles and nanostructures: a review, J. Taiwan Inst. Chem. Eng. 149 (2023), 105010, https://doi.org/10.1016/j.jtice.2023.105010.

[10] D. Gupta, A. Thakur, T.K. Gupta, Green and sustainable synthesis of nanomaterials: recent advancements and limitations, Environ. Res. (2023), 116316, https://doi.org/10.1016/j.envres.2023.116316.

[11] S.F. Tehrani, P. Bharadwaj, J.L. Chain, V.G. Roullin, Purification processes of polymeric nanoparticles: how to improve their clinical translation? J. Contr. Release 360 (2023) 591–612, https://doi.org/10.1016/j.jconrel.2023.06.038.

[12] G.M. Nair, T. Sajini, B. Mathew, Advanced green approaches for metal and metal oxide nanoparticles synthesis and their environmental applications, Talanta Open 5 (2022), 100080, https://doi.org/10.1016/j.talo.2021.100080.

[13] J. Jeevanandam, S.F. Kiew, S. Boakye-Ansah, S.Y. Lau, A. Barhoum, M.K. Danquah, J. Rodrigues, Green approaches for the synthesis of metal and metal oxide nanoparticles using microbial and plant extracts, Nanoscale 14 (2022) 2534–2571, https://doi.org/10.1039/D1NR08144F.

[14] N.M. Ishak, S.K. Kamarudin, S.N. Timmiati, Green synthesis of metal and metal oxide nanoparticles via plant extracts: an overview, Mater. Res. Express 6 (2019), 112004.

[15] H. Zhao, M. Maruthupandy, F.A. Al-mekhlafi, G. Chackaravarthi, G. Ramachandran, C.K. Chelliah, Biological synthesis of copper oxide nanoparticles using marine endophytic actinomycetes and evaluation of biofilm producing bacteria and A549 lung cancer cells, J. King Saud Univ. Sci. 34 (2022), 101866, https://doi.org/10.1016/j.jksus.2022.101866.

[16] M. Sulak, B. Kavakcıoğlu Yardımcı, B. The green synthesis of MgO nanoparticles using dried jujube fruit extract and their anti-yeast activity against Saccharomyces cerevisiae, Inorg. Nano-Metal Chem. 52 (2022) 653–660, https://doi.org/10.1080/24701556.2021.1956970.

[17] V. Soni, A. Khosla, P. Singh, V.H. Nguyen, Q. Van Le, R. Selvasembian, C.M. Hussain, S. Thakur, P. Raizada, Current perspective in metal oxide based photocatalysts for virus disinfection: a review, J. Environm. Manag. 308 (2022), 114617, https://doi.org/10.1016/j.jenvman.2022.114617.

[18] A.M. Shafey, Green synthesis of metal and metal oxide nanoparticles from plant leaf extracts and their applications: a review, Green Process. Syn. 9 (2020) 304–339, https://doi.org/10.1515/gps-2020-0031.

[19] M.S. Samuel, M. Ravikumar, J.A. John, E. Selvarajan, H. Patel, P.S. Chander, J. Soundarya, S. Vuppala, R. Balaji, N. Chandrasekar, A review on green synthesis of nanoparticles and their diverse biomedical and environmental applications, Catalysts 12 (2022) 459. https://www.mdpi.com/2073-4344/12/5/459#.

[20] A. Balciunaitiene, M. Liaudanskas, V. Puzerytė, J. Viskelis, V. Janulis, P. Viskelis, E. Griskonis, V. Jankauskaite, Eucalyptus globulus and Salvia officinalis extracts mediated green synthesis of silver nanoparticles and their application as an antioxidant and antimicrobial agent, Plants 11 (2022) 1085, https://doi.org/10.3390/plants11081085.

[21] M. Jakovljevic, S. Jokic, M. Molnar, M. Jasic, J. Babic, H. Jukic, Banjari, Bioactive profile of various Salvia officinalis L. preparations, Plants 8 (2019) 55, https://doi.org/10.3390/plants8030055.

[22] A.H. Alrajhi, N.M. Ahmed, Green synthesis of zinc oxide nanoparticles using Salvia *officinalis* extract, in: Handbook of Green and Sustainable Nanotechnology: Fundamentals, Develop. Appl., Springer International Publishing, Cham, 2023, pp. 1–21, https://doi.org/10.1007/978-3-030-69023-6_44-1.

[23] D.K. Takcı, M.S. Ozdenefe, S. Genc, Green synthesis of silver nanoparticles with an antibacterial activity using *Salvia officinalis* aqueous extract, J. Cry. Growth (2023), 127239, https://doi.org/10.1016/j.jcrysgro.2023.127239.

[24] M. Liaudanskas, V. Puzeryte, J. Viškelis, V. Janulis, P. Viskelis, E. Griskonis, V. Jankauskaite, Eucalyptus globulus and *Salvia officinalis* extracts mediated green synthesis of silver nanoparticles and their application as an antioxidant and antimicrobial agent, Plants 11 (2022) 1085, https://doi.org/10.3390/plants11081085.

[25] S. Masturah binti Fakhruddin, K. Ino, K.Y. Inoue, Y. Nashimoto, H. H. Shiku, Bipolar electrode-based electrochromic devices for analytical applications–A review, Electroanalysis 34 (2022) 212–226, https://doi.org/10.1002/elan.202100153.

[26] H. Tang, Q. Chen, S. Lu, X. Li, H. Li, Y. Wang, K. Wang, Q. Zhou, Z. Wang, Naphthyl-modified graphitic carbon nitride: preparation and application in light-emitting diodes, J. Lumin. 244 (2022), 118734, https://doi.org/10.1016/j.jlumin.2022.118734.

[27] X. Hong, M. Dai, C. Ke, G. Wang, C. Qian, C. Zhu, Graphite oxide/reduced graphite oxide surface modified carbon fiber reinforced composites for deicing and electromagnetic interference shielding, J. Mater. Sci. Mater. Electron. 34 (2023) 1–13, https://doi.org/10.1007/s10854-022-09424-x.

[28] L. Yuan, J. Xu, Z. Yang, Q. Su, J. Li, Zinc oxide anode modified with zeolite imidazole structure achieve stable circulation for zinc–nickel secondary battery, J. Power Sour. 517 (2022), 230696, https://doi.org/10.1016/j.jpowsour.2021.230696.

[29] J. Huang, W. Wu, R. Zhang, G. Lu, B. Chen, Z. Chen, C. Gui, Novel electrode material using electroless nickel plating for triboelectric nanogenerator: study of the relationship between electrostatic-charge density and strain in dielectric material, Nano Energy 92 (2022), 106734, https://doi.org/10.1016/j.nanoen.2021.106734.

[30] D. Garg, M. Singh, N. Verma, Review on recent advances in fabrication of enzymatic and chemical sensors for hypoxanthine, Food Chem. 375 (2022), 131839, https://doi.org/10.1016/j.foodchem.2021.131839.

[31] A. Dinu, C. Apetrei, A review of sensors and biosensors modified with conducting polymers and molecularly imprinted polymers used in electrochemical detection of amino acids: phenylalanine, tyrosine, and tryptophan, Int. J. Mol. Sci. 23 (2022) 1218, https://doi.org/10.3390/ijms23031218.

[32] M.M. Rashidi, M. Alhuyi Nazari, I. Mahariq, N. Ali, Modeling and sensitivity analysis of thermal conductivity of ethylene glycol-water based nanofluids with alumina nanoparticles, Exp. Tech. 47 (2023) 83–90, https://doi.org/10.1007/s40799-022-00567-4.

[33] A. Alaghmandfard, K. Ghandi, A comprehensive review of graphitic carbon nitride (g-C3N4)–metal oxide-based nanocomposites: potential for photocatalysis and sensing, Nanomaterials 12 (2022) 294, https://doi.org/10.3390/nano12020294.

[34] V. Mani, K. Krishnaswamy, F.S. Arockiasamy, T.S. Manickam, Mechanical and dielectric properties of Cissus Quadrangularis fiber-reinforced epoxy/TiB_2 hybrid composites, Int. Polym. Process. (0) (2023), https://doi.org/10.1515/ipp-2022-4321.

[35] J. Iyyadurai, F.S. Arockiasamy, T.S. Manickam, I. Suyambulingam, S. Siengchin, M. Appadurai, E. Raj, Revolutionizing Polymer Composites: Boosting Mechanical Strength, Thermal Stability, Water Resistance, and Sound Absorption of Cissus Quadrangularis Stem Fibers with Nano Silica, 2023, pp. 1–13, https://doi.org/10.1007/s12633-023-02510-7. Silicon.

[36] S. Davoodi, M. Al-Shargabi, D.A. Wood, V.S. Rukavishnikov, K.M. Minaev, Experimental and field applications of nanotechnology for enhanced oil recovery purposes: a review, Fuel 324 (2022), 124669, https://doi.org/10.1016/j.fuel.2022.124669.

[37] A. Felix Sahayaraj, H. Joy Prabu, J. Maniraj, M. Kannan, M. Bharathi, P. Diwahar, J. Salamon, Metal–organic frameworks (MOFs): the next generation of materials for catalysis, gas storage, and separation, J. Inorg. Organomet. Polym. Mater. (2023) 1–25, https://doi.org/10.1007/s10904-023-02657-1.

[38] C. Lete, A.M. Spinciu, M.G. Alexandru, J. Calderon Moreno, S.A. Leau, M. Marin, D. Visinescu, Copper (II) oxide nanoparticles embedded within a PEDOT matrix for hydrogen peroxide electrochemical sensing, Sensors 22 (2022) 8252, https://doi.org/10.3390/s22218252.

[39] S.A. Al-Tamimi, Biogenic green synthesis of metal oxide nanoparticles using oat biomass for ultrasensitive modified polymeric sensors, Green Chem. Lett. Rev. 14 (2021) 166–179, https://doi.org/10.1080/17518253.2021.1895326.

[40] N.C. Joshi, Leaves extract-based biogenic synthesis of cupric oxide nanoparticles, characterizations, and antimicrobial activity, Asian. J. Pharm. Clin. Res. 12 (2019) 288–291, https://doi.org/10.22159/ajpcr.2019.v12i8.34182. Y.A.S.H.W.A.N.I. Prakash.

[41] S.A. Akintelu, A.S. Folorunso, F.A. Folorunso, A.K. Oyebamiji, Green synthesis of copper oxide nanoparticles for biomedical application and environmental remediation, Heliyon 6 (2020), e04508, https://doi.org/10.1016/j.heliyon.2020.e04508.

[42] J. Gangwar, B.K. Gupta, A.K. Srivastava, Prospects of emerging engineered oxide nanomaterials and their applications, Def. Sci. J. 66 (2016) 323–340.

[43] A.M. Al-Mohaimeed, G.A. Mostafa, M.F. El-Tohamy, New construction of functionalized CuO/Al_2O_3 nanocomposite-based polymeric sensor for potentiometric estimation of naltrexone hydrochloride in commercial formulations, Polymers 13 (2021) 4459, https://doi.org/10.3390/polym13244459.

[44] D. Wang, D. Zhang, M. Tang, H. Zhang, T. Sun, C. Yang, R. Mao, K. Li, J. Wang, Ethylene chlorotrifluoroethylene/hydrogel-based liquid-solid triboelectric nanogenerator driven self-powered MXene-based sensor system for marine environmental monitoring, Nano Energy 100 (2022), 107509, https://doi.org/10.1016/j.nanoen.2022.107509.

[45] T. Imamura, W. Gonoi, M. Hori, Y. Ueno, N. Narang, H. Onoda, S. Tanaka, M. Nakamura, N. Kataoka, R. Ushijima, M. Sobajima, Validation of noninvasive remote dielectric sensing system to quantify lung fluid levels, J. Clin. Med. 11 (2022) 164, https://doi.org/10.3390/jcm11010164.

[46] T. Bhatta, P. Maharjan, K. Shrestha, S. Lee, M. Salauddin, M.T. Rahman, S.S. Rana, S. Sharma, C. Park, S.H. Yoon, J.Y. Park, A Hybrid self-powered arbitrary wave motion sensing system for real-time wireless marine environment monitoring application, Adv. Energy Mater. 12 (2022), 2102460, https://doi.org/10.1002/aenm.202102460.

[47] Y. Zhang, C. Wang, F. Liu, X. Sun, X. Guo, L. Zhao, G. Lu, 3-Aminopropyltriethoxysilane functionalized ZnO materials for improving the gas sensitivity to 2-butanone, Sens. Actuators B: Chem. 363 (2022), 131845, https://doi.org/10.1016/j.snb.2022.131845.

[48] D. Lu, Z. Yao, L. Jiao, M. Waheed, Z. Sun, L. Zhang, Separation mechanism, selectivity enhancement strategies and advanced materials for mono-/multivalent ion-selective nanofiltration membrane, Adv. Membr. 2 (2022), 100032, https://doi.org/10.1016/j.advmem.2022.100032.

[49] S.S. Alterary, M.F. El-Tohamy, Advanced functionalized CeO_2/Al_2O_3 Nanocomposite sensor for determination of opioid medication tramadol hydrochloride in pharmaceutical formulations, Nanomaterials 12 (2022) 1373, https://doi.org/10.3390/nano12081373.

[50] S.R. Cho, D.H. Kim, M. Jeon, P. Rani, M. Gyeon, Y. Kim, M.K. Jo, S. Song, J.Y. Park, J. Kim, I.D. Kim, Overlaying monolayer metal–organic framework on $PtSe_2$-based gas sensor for tuning selectivity, Adv. Funct. Mater. 32 (2022), 2207265, https://doi.org/10.1002/adfm.202207265.

[51] M.F. Yam, Y.C. Loh, C.W. Oo, R. Basir, Overview of neurological mechanism of pain profile used for animal "pain-like" behavioral study with proposed analgesic pathways, Int. J. Mol. Sci. 21 (2020) 4355, https://doi.org/10.3390/ijms21124355.

[52] S. Majumdar, S. Roy, R.R. Llinás, Study of the bacterial" conversations" and pattern formation in the quorum sensing system using numerical simulation, J. Hum. Earth Future 3 (2022) 30–45.

[53] S. Smieszek, M.H. Polymeropoulos, Study of regions of homozygosity (ROH) patterns to evaluate the use of dogs' genome in human drug development, J. Hum. Earth Future 3 (2022) 22–29.

[54] A. Kubica-Cielinska, M. Czapla, R. Juárez-Vela, C.I. Tejada-Garrido, M. Zielinska, Comparison of side effects of nalbuphine and morphine in the treatment of pain in children with cancer: a Prospective Study, Cancers14 (2022) 3617, https://doi.org/10.3390/cancers14153617.

[55] A. Khan, M. Asghar, M. Yaqoob, Determination of nalbuphine hydrochloride in pharmaceutical formulations using diperiodatoargentate (III)-rhodamine-B chemiluminescence system by flow injection analysis, Anal. Sci. 36 (2022) 1223–1227, https://doi.org/10.2116/analsci.20P126.

[56] A.M. El-Didamony, I.I. Ali, New spectrofluorimetric and spectrophotometric methods for the determination of the analgesic drug, nalbuphine in pharmaceutical and biological fluids, Luminescence 28 (2013) 745–750, https://doi.org/10.1002/bio.2428.

[57] H.J. Wang, C.H. Hsiong, L.H. Pao, W.L. Chang, L.J. Zhang, M.J. Lin, S.T. Ho, P.W. Huang, O.Y.P. Hu, New finding of nalbuphine metabolites in men: NMR spectroscopy and UPLC–MS/MS spectrometry assays in a pilot human study, Metabolomics 10 (2014) 709–718, https://doi.org/10.1007/s11306-013-0605-y.

[58] N.F. Atta, A. Galal, S.H. Hassan, Ultrasensitive determination of nalbuphine and tramadol narcotic analgesic drugs for postoperative pain relief using nano-cobalt oxide/ionic liquid crystal/carbon nanotubes-based electrochemical sensor, J. Electroanal. Chem. 839 (2019) 48–58, https://doi.org/10.1016/j.jelechem.2019.03.002.

[59] D.P. Costanza, J.B. Darrow, A.B. Yost, J.B. Severt, A review of analytical methods used to study generational differences: strengths and limitations, Work, Aging Retir. 3 (2017) 149–165, https://doi.org/10.1093/workar/wax002.

[60] I.H.T. Guideline, R1, in: Validation Of Analytical Procedures: Text And Methodology Q2, 2005, p. 1, 05.

[61] V.D. Mote, S.D. Lokhande, L.H. Kathwate, M.B. Awale, Y. Sudake, Structural, optical and magnetic properties of Mn-doped CuO nanoparticles by coprecipitation method, Mater. Sci. Eng. B 289 (2023), 116254, https://doi.org/10.1016/j.mseb.2022.116254.

[62] S.Y. Al Omar, A.M. Al-Mohaimeed, M.F. El-Tohamy, Ultrasensitive functionalized CeO_2/ZnO nanocomposite sensor for determination of a prohibited narcotic in sports pethidine hydrochloride, Heliyon 9 (2023), e15793, https://doi.org/10.1016/j.heliyon.2023.e15793.

[63] S. Sarkar, E. Guibal, F. Quignard, A.K. SenGup, Polymer-supported metals and metal oxide nanoparticles: synthesis, characterization, and applications, J. Nanopart. Res. 11 (2012) 715.

[64] R.A. Al-Sabbah, S.A. Al-Tamimi, N.A. Alarfaj, M.F. El-Tohamy, Modified millet extract-mediated NiO/CaO Nanocomposite potentiometric sensor for monitoring of ciprofloxacin in commercial products, Inter. J. Electrochem. Sci. 18 (2023), 100284, https://doi.org/10.1016/j.ijoes.2023.100284.

[65] M. Logash, P. Pokotylo, B. Zboina, R.B. Stępien, Nalbuphine: some aspects of the research and applications, Med. Stud. 33 (2017) 146–154, https://doi.org/10.5114/ms.2017.68710.

[66] M.D. Mot, S. Gavrilaș, A.I. Lupitu, C. Moisa, D. Chambre, D.M. Tit, M.A. Bogdan, A.M. Bodescu, L. Copolovici, D.M. Copolovici, S.G. Bungau, *Salvia officinalis* L. Essential oil: characterization, antioxidant properties, and the effects of aromatherapy in adult patients, Antioxidants 11 (2022) 808, https://doi.org/10.3390/antiox11050808.

[67] P. Manogar, J.E. Morvinyabesh, P. Ramesh, G.D. Jeyaleela, V. Amalan, J.S. Ajarem, A.A. Allam, J.S. Khim, N. Vijayakumar, Biosynthesis and antimicrobial activity of aluminium oxide nanoparticles using Lyngbya majuscula extract, Mater. Lett. 311 (2022), 131569, https://doi.org/10.1016/j.matlet.2021.131569.

[68] S.A. Akintelu, A.S. Folorunso, F.A. Folorunso, A.K. Oyebamiji, Green synthesis of copper oxide nanoparticles for biomedical application and environmental remediation, Heliyon 6 (2020), e04508, https://doi.org/10.1016/j.heliyon.2020.e04508.

[69] X. Yue, T. Zhang, D. Yang, F. Qiu, J. Rong, J. Xu, J. Fang, The synthesis of hierarchical porous Al_2O_3/acrylic resin composites as durable, efficient and recyclable absorbents for oil/water separation, Chem. Eng. J. 309 (2017) 522–531, https://doi.org/10.1016/j.cej.2016.10.049.

[70] B.S. Hulbert, W.M. Kriven, Specimen-displacement correction for powder X-ray diffraction in Debye–Scherrer geometry with a flat area detector, J. Appl. Cryst. 56 (2023) 160–166, https://doi.org/10.1107/S1600576722011360.

[71] G.A. Mostafa, M.F. El-Tohamy, H. Alrabiah, Prospective of agro-waste husks for biogenic synthesis of polymeric-based CeO2/NiO nanocomposite sensor for determination of mebeverine hydrochloride, Molecules 28 (2023), https://doi.org/10.3390/molecules28052095, 2095.

[72] P. Mishra, U. Singh, C.M. Pandey, P. Mishra, G. Pandey, Application of student's t-test, analysis of variance, and covariance, Annal. Card. Anaesth. 22 (2019) 407.

[73] K.A.S. Attia, M.W. Nassar, A. El-Olemy, Stability-Indicating spectrophotometric determination of nalbuphine hydrochloride using first derivative of ratio spectra and ratio difference methods, Methods 7 (2014) 13.

[74] F. Belal, F. Ibrahim, Z.A. Sheribah, H. Alaa, New spectrophotometric/chemometric assisted methods for the simultaneous determination of imatinib, gemifloxacin, nalbuphine and naproxen in pharmaceutical formulations and human urine, Spectrochim. Acta Part A: Mol. Biomol. Spectr. 198 (2018) 51–60, https://doi.org/10.1016/j.saa.2018.02.048.

[75] A.M. El-Didamony, I.I. Ali, New spectrofluorimetric and spectrophotometric methods for the determination of the analgesic drug, nalbuphine in pharmaceutical and biological fluids, Luminescence 28 (2013) 745–750, https://doi.org/10.1002/bio.2428.

[76] A. Khan, M. Asghar, M. Yaqoob, Determination of nalbuphine hydrochloride in pharmaceutical formulations using diperiodatoargentate (III)-rhodamine-B chemiluminescence system by flow injection analysis, Anal. Sci. 36 (2020) 1223–1227, https://doi.org/10.1007/s40242-020-0339-0.
[77] K.A. Attia, M.W. Nassar, A. El-Olemy, Stability-indicating HPLC method for determination of nalbuphine hydrochloride, Int. J. Res. Pharmaceut. Biomed. Sci. 1 (2014) 15–22.
[78] N.F. Atta, A. Galal, S.H. Hassan, Ultrasensitive determination of nalbuphine and tramadol narcotic analgesic drugs for postoperative pain relief using nano-cobalt oxide/ionic liquid crystal/carbon nanotubes-based electrochemical sensor, J. Electroanal. Chem. 839 (2019) 48–58, https://doi.org/10.1016/j.jelechem.2019.03.002.
[79] T. Tavana, A.R. Rezvani, H. Karimi-Maleh, Pt-Pd-doped NiO nanoparticle decorated at single-wall carbon nanotubes: an excellent, powerful electrocatalyst for the fabrication of an electrochemical sensor to determine nalbuphine in the presence of tramadol as two opioid analgesic drugs, J. Pharm. Biomed. Anal. 189 (2020), 113397, https://doi.org/10.1016/j.jpba.2020.113397.
[80] S.S. Hassan, A.H. Kamel, M.A. Fathy, A novel screen-printed potentiometric electrode with carbon nanotubes/polyaniline transducer and molecularly imprinted polymer for the determination of nalbuphine in pharmaceuticals and biological fluids, Anal. Chim. Acta 1227 (2022), 340239, https://doi.org/10.1016/j.aca.2022.340239.